Hydrometallurgy 96 (2009) 132–139

Contents lists available at ScienceDirect

Hydrometallurgy

journal homepage: www.elsevier.com/locate/hydromet

Experimental study of pyrite–galena mixed potential in a flowing system and its applied implications

Qingyou Liu, Heping Li *, Li Zhou

Laboratory for Study of the Earth's Interior and Geofluids, Institute of Geochemistry, Chinese Academy of Sciences, Guiyang 550002, China

ARTICLE INFO

Article history:
Received 29 April 2008
Received in revised form 16 September 2008
Accepted 16 September 2008
Available online 25 September 2008

Keywords:
Unstrained pyrite
Strained pyrite
Galena
Galvanic interaction
Flowing system
Corrosion current density
Mixed potential

ABSTRACT

A three-electrode system was adopted to investigate the corrosion current density and mixed potential of unstrained pyrite–galena and strained pyrite–galena galvanic cells in a flowing system. The results showed that when present in the same solution, strained pyrite produces a lower electrode potential than that of the galena electrode because of its strain energy; moreover, increasing the sodium sulfate solution concentration causes only slight fluctuations in the corrosion current density and mixed potential, while these values clearly increased with increasing ferric sulfate solution concentrations. In addition, for the sodium sulfate solution or ferric sulfate electrolyte, the faster the flow rate, the bigger the corrosion current density and the more positive the mixed potential of the galvanic cell. The experimental results are significant for hydrometallurgy and for controlling environmental pollution in mining activities. By using the galvanic model, mixed potential theory and the Butler–Volmer equation, the experimental results were explained theoretically.

1. Introduction

Galvanic interactions are known to occur between conducting minerals and play a significant role in hydrometallurgical applications (Majima and Peter, 1968; Chandraprabha et al., 2004; Cruz et al., 2005; Seke and Pistorius, 2006), flotation (Rao and Finch, 1988; Kelebek et al., 1996; Zhang et al., 1997; Ekmekçi and Demirel, 1997; Huang and Grano, 2005), leaching (Mehta and Murr, 1983; Abraitis et al., 2003a,b; Akcil and Ciftci, 2003), supergene enrichment of sulfide ore deposits (Thornber, 1975a,b; Sato, 1992), environment governance (Alpers and Blowes, 1994), and geochemical processes (Sikka et al., 1991; Banfield, 1997).

Pyrite and galena are the most common sulfide minerals and are broadly found in igneous rocks, sedimentary and hydrothermal deposits. Pyrite, as the commercial source of sulfuric acid, is presently mined as a source of gold, while galena, the primary ore mineral of lead, has been harvested for its lead content from as early as 3000 BC, and is mined as a source of silver. The galvanic interaction between pyrite and galena is one of the most representative and most influential galvanic interactions between two sulfide minerals in nature and in industry. As a result, many galvanic studies of the pyrite–galena couple have been published (Pecina et al., 2006; Chernyshova, 2003; Peng et al., 2003; Pecina-Treviño et al., 2003). Pecina-Treviño et al. (2003) studied the galvanic interaction of synthetic mixtures of galena and pyrite affecting their flotation response; they suggested that galena–pyrite galvanic contact lowers the adsorption of lead species onto pyrite, compared to that observed with pyrite alone. The collector chemisorbs onto galena, forming a layer of low electroactivity that slows down the dissolution of the mineral but does not completely prevent galvanic interaction with pyrite. Holmes and Crundwell (1995) studied the galvanic interaction between pyrite and galena based on thermodynamic and kinetic parameters, and observed mathematical agreement with experimentally measured galvanic currents. Abraitis et al. (2003a,b) investigated the major sulfide ore minerals in acid leaching and reported that galvanic interactions (including the pyrite–galena couple) could substantially increase the leaching rate of one or both of the minerals that constitute the galvanic cell, depending on the electrochemical characteristics of the minerals.

Previous studies on pyrite–galena galvanic corrosion were mostly carried out without stress. However, the fact is that pyrite and galena are always subject to stress action, whether being exploited by humans or as a result of normal geochemical processes. Stress causes a conversion of the strain energy into electrochemical energy, which thereby changes the electrode potential, and furthermore has a major influence on the galvanic corrosion of sulfide minerals. Other previous studies on pyrite–galena galvanic

* Corresponding author.
E-mail address: liheping123@yahoo.com (H. Li).

0304-386X/$ – see front matter © 2008 Elsevier B.V. All rights reserved.
doi:10.1016/j.hydromet.2008.09.002

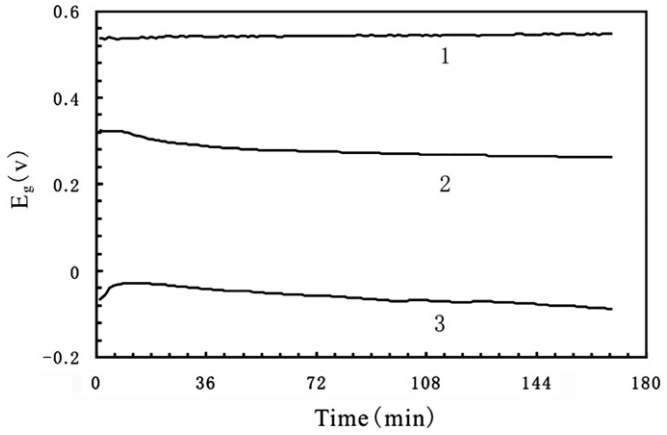

Fig. 1. Variations in potential with time in a 0.01 mol/L $Fe_2(SO_4)_3$ solution: (1) unstrained pyrite, (2) galena, and (3) natural strained pyrite.

corrosion focused on quietly aqueous systems and rarely referred to flowing aqueous systems. However, in nature, these sulfide minerals are often found in flowing aqueous systems environments. In mine environments, for instance, pyrite and galena are often found under flowing surface water, ground water and raining water. Experimental studies under flowing aqueous systems are therefore of direct relevance to controlling the environmental pollution of mines.

In other words, an experimental study of the pyrite–galena galvanic in a flowing system, with or without stress action, can provide an experimental basis for sulfide's hydrometallurgy, and has direct significance for controlling environmental pollution in mining activities. The objective of this paper is to investigate the galvanic interaction of unstrained and strained pyrite with galena.

2. Experimental

2.1. Materials and apparatus

Natural minerals were used: unstrained pyrite and natural strained pyrite from a large piece of natural pyrite mineral adjacent part, the Dongchuan copper deposit of Yunnan Province, China. The electron microprobe analysis confirmed Fe and S (wt.%) are 46.89% and 52.96%, respectively; galena from the Huize Pb–Zn deposit of Yunnan Province, China. It's Pb, S and Zn (wt.%) were 86.53%, 13.39% and 0.0064%, respectively.

The "natural strained pyrite" referred to here is pyrite whose surface had natural cracks before it was mined from the deposit: in other words, it has crystal defects due to natural stress action from long geological processes.

Samples were cut from large pieces of the natural minerals and worked with emery papers into the shape of a cylinder 8 mm in diameter and several centimetres tall. Then, a copper wire was soldered onto one end surface of each cylinder. The mineral electrodes were mounted in a properly-sized PTFE, followed by injection of epoxy resin for sealing and fixing. $1^{\#}$–$5^{\#}$ metallographic abrasive papers were used to polish the working surfaces of the electrodes. Optical microscopy was used to observe the existence of superficial phases of the surfaces; observed results confirmed that the three electrodes corresponded to respective sulfide minerals. Immediately before the experiment, the surfaces of the minerals were polished using a 3 micron abrasive paper and then washed with acetone until clean.

The unstrained pyrite, natural strained pyrite and galena electrode potentials were measured through a standard two-electrode system, where a saturated calomel reference (SCE) electrode was used as the reference electrode; simulated mineral stress experiments were carried out on an electronic universal testing machine controlled by computer. The testing machine offered experimental required rapid, continuous different axial stresses.

A standard flow circuit set-up was adopted in the flowing experiment. In or to contrast, unstrained pyrite, galena and SCE three-electrode composed one cell; strained pyrite, galena and SCE three-electrode composed another cell. All potentials recorded in this study were relative to the SCE. Two HP-34401A high precision digital multimeters connected to a computer were used to measure the corrosion current density and mixed potential.

2.2. Experimental conditions

Previous reports have shown: (1) In a metal sulfide mine, the mine drainage usually bears Fe^{3+} of different concentrations, and its pH ranges from 2 to 4 (Elliott et al., 1998); (2) The flow rate of mine media (e.g., mountainous brook) is usually larger than 0.3 m/s (Merkblatt ATV-DVWK M 153, 2000). In view of these conditions, various flowing experiments were carried out, including for control of Na^+ and Fe^{3+} concentrations and the flow rates of the solutions.

All flow experiments were carried out in 10 L glass vessels with a 5 L solution, at a temperature of 25±0.2 °C. The dissolved O_2 concentrations were maintained at about 8.0–8.5 mg/L, and equilibrated in air. Analytical grade ferric sulfate and sodium sulfate were used in the experimental investigation. Sulfuric acid (98%) was used to obtain the desired pH (in this work we controlled pH=3.78) for each experiment.

3. Results

3.1. Unstrained pyrite, natural strained pyrite and galena potentials

Fig. 1 shows the variations in potential with time for unstrained pyrite, natural strained pyrite and galena in a 0.01 mol/L $Fe_2(SO_4)_3$ solution. From this figure we can see that the potential of the unstrained pyrite electrode is higher than that of the potential of the galena electrode, which is in agreement with previous literature reported that pyrite is the most noble sulfide (Natarajan and

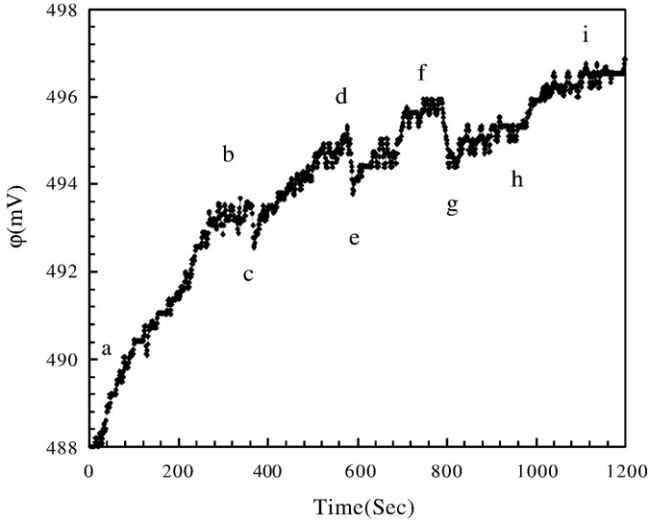

Fig. 2. Variations in pyrite electrode potential under rapid, continuously varying axial stresses in a 0.01 mol/L sodium sulfate solution. [stress: ab—0 MPa; cb—15 MPa; ef—30 MPa; gh—45 MPa; hi—0 MPa.]

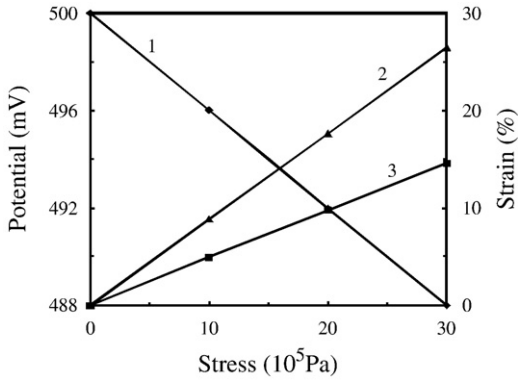

Fig. 3. Chart of pyrite potential-stress–strain. [(1) axial stress–pyrite potential, (2) axial stress–axial strain, and (3) axial stress–lateral strain.]

Iwasaki, 1972); however, when the pyrite has natural interstices, its electrode potential falls below that of the galena electrode.

3.2. Effect of stress

Fig. 2 depicts the variations in pyrite electrode potential under rapid and continuously varying axial stress in a 0.01 mol/L sodium sulfate solution. Combining stress and strain conditions in the experiment allowed us to derive a stress–strain-potential chart (Fig. 3).

3.3. Effect of sodium sulfate concentration

Fig. 4 depicts the variations in the corrosion current density and mixed potential of unstrained pyrite–galena and natural strained pyrite–galena galvanic in different sodium sulfate concentration solutions. This figure shows that a tenfold increase in Na^+ concentration, whether due to unstrained pyrite–galena or natural strained pyrite–galena galvanic interaction, leads to only moderate fluctuations in the corrosion current density and mixed potential.

3.4. Effect of ferric sulfate concentration

Fig. 5 depicts the variations in the corrosion current density and mixed potential of unstrained pyrite–galena and natural strained pyrite–galena galvanic in different ferric sulfate concentration solutions. This figure shows that when the concentrations of Fe^{3+} varied from 0 to 0.001 mol/L, the galvanic i_g obviously increased. Unstrained pyrite–galena i_g varied from 0.525 to 2.25 uA/cm^2, whereas natural strained pyrite–galena i_g varied only from 0.262 to 0.381 uA/cm^2. The greater the concentration of Fe^{3+} (from 0.001 to 0.1 mol/L), the higher the corrosion current density (unstrained pyrite–galena i_g varied from 2.25 to 4.50 uA/cm^2 and natural strained pyrite–galena i_g varied from 0.381 to 0.762 uA/cm^2); at the same time, with increasing concentration of Fe^{3+}, the mixed potential also increased (E_g varied from about 0.148 to 0.277 V and 0.273 to 0.346 V, respectively).

3.5. Effect of electrolyte flow rates

Fig. 6 depicts the variations in the corrosion current density and mixed potential of unstrained pyrite–galena and natural strained pyrite–galena galvanic in different flow rate sodium sulfate solutions. Fig. 7 depicts the variations in the corrosion current density and mixed potential of unstrained pyrite–galena and natural strained pyrite–galena galvanic in different flow rate ferric sulfate solutions.

Figs. 6 and 7 show results for when the solution flow rate increased by ten times: whether due to unstrained pyrite–galena or to natural strained pyrite–galena galvanic interaction, the faster the flow rate, the bigger the corrosion current density (with the

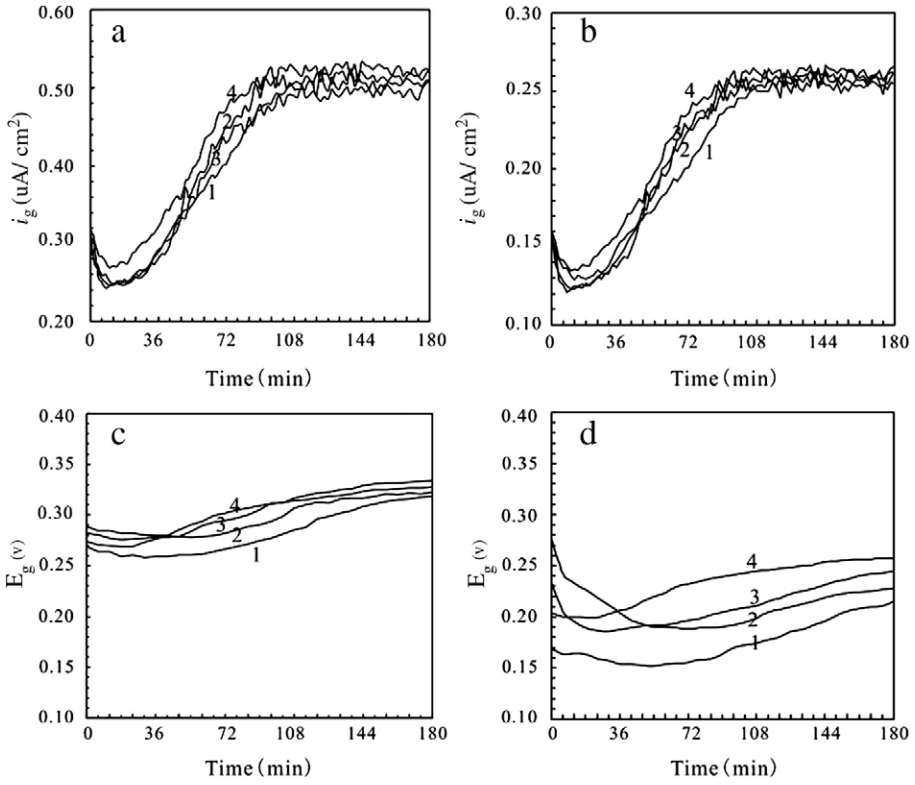

Fig. 4. Variations in i_g and E_g with time for different sodium sulfate concentrations. [298 K, pH = 3.78, (1) 0 mol/L (2) 0.0001 mol/L (3) 0.001 mol/L (4) 0.01 mol/L. a,c—unstrained pyrite–galena galvanic, flow rate 0.36 m/s; b,d—strained pyrite–galena galvanic, flow rate 0.24 m/s.]

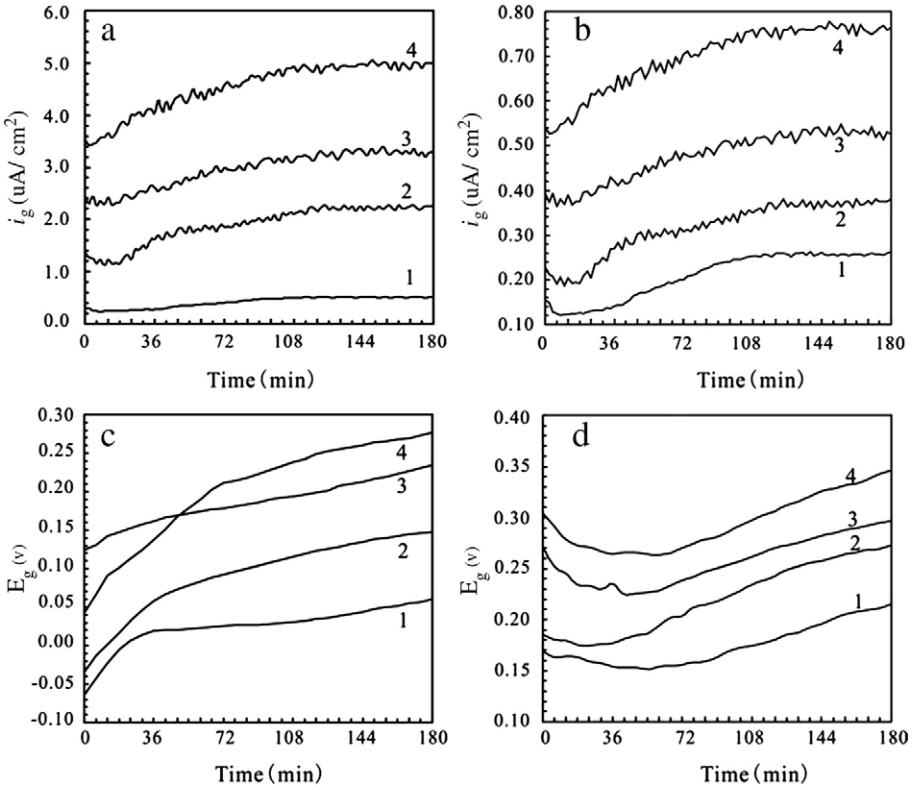

Fig. 5. Variations in i_g and E_g with time for different ferric sulfate concentrations. [298 K, pH=3.78, (1) 0 mol/L (2) 0.0001 mol/L (3) 0.001 mol/L (4) 0.01 mol/L. a,c—unstrained pyrite–galena galvanic, flow rate 0.36 m/s; b,d—strained pyrite–galena galvanic, flow rate 0.24 m/s.]

sodium sulfate solution, galvanic i_g varied about from 0.247 to 0.532 uA/cm^2 and 0.212 to 0.395 uA/cm^2, respectively; for the ferric sulfate solution, galvanic i_g varied from 0.256 to 0.490 uA/cm^2 and 0.256 to 0.560 uA/cm^2, respectively), and the more positive the mixed potential (with the sodium sulfate solution, E_g varied about from 0.173 to 0.328 V and 0.193 to 0.303 V, respectively,, and for the

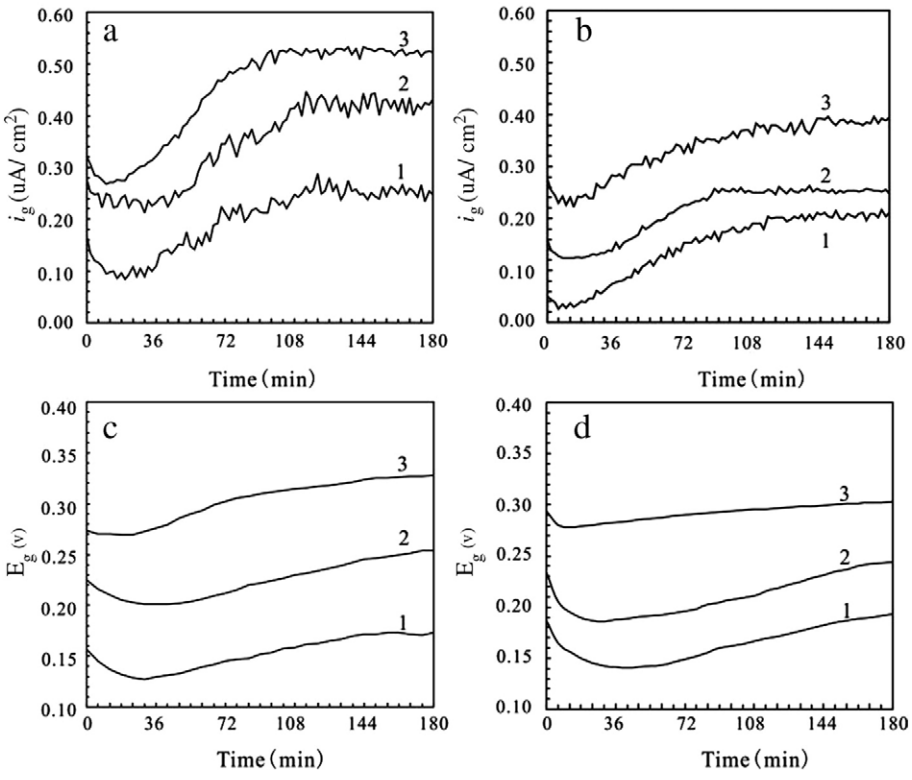

Fig. 6. Variations in i_g and E_g with time for different flow rates and sodium sulfate concentrations. [298 K, pH=3.78, Na^+ 0.01 mol/L, a,c—unstrained pyrite–galena galvanic (1) 0.06 m/s; (2) 0.24 m/s; (3) 0.36 m/s. b,d—strained pyrite–galena galvanic (1) 0.06 m/s; (2) 0.24 m/s; (3) 0.42 m/s.]

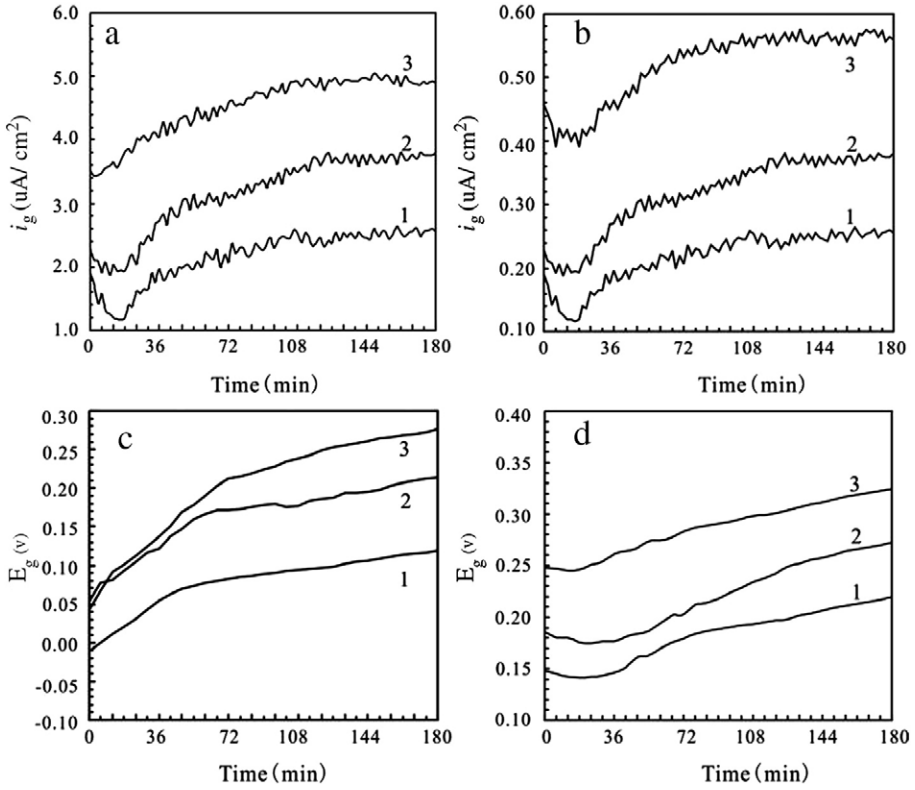

Fig. 7. Variations in i_g and E_g with time for different flow rates and ferric sulfate concentrations. [298 K, pH = 3.78, Fe^{3+} 0.01 mol/L, a,c—unstrained pyrite–galena galvanic (1) 0.06 m/s; (2) 0.24 m/s; (3) 0.36 m/s. b,d—strained pyrite–galena galvanic (1) 0.06 m/s; (2) 0.24 m/s; (3) 0.42 m/s.]

ferric sulfate solution, E_g varied from about 0.119 to 0.227 V and 0.219 to 0.324 V, respectively).

4. Discussion

4.1. Theoretical explanation for the natural strained pyrite and stress electrode potential

Natural cracks on a pyrite surface will induce stress, increase activity energy increase and facilitate chemical reactions (Lasaga and Blum, 1986; Mckibben and Barnes, 1986). According to the electrochemistry principle (Li, 1999), the pyrite (or galena) potential (φ_H^{MS}) consists of two parts: the phase boundary potential between the pyrite (or galena) and the solution ($\Delta^M\Phi^S$), and the pyrite (or galena) contact potential (Φ_0).

$$\varphi_H^{MS} = \Delta^M\Phi^S - \Phi_0. \tag{1}$$

When the pyrite (or galena) and solution phases are at equilibrium, the electrochemical potentials of the two phases are equal:

$$\overline{\mu^M} = \overline{\mu^s} \Rightarrow \mu^M + ZF\Phi^M = \mu^s + ZF\Phi^s \Rightarrow$$
$$\mu^M - \mu^s = ZF\Phi^s - ZF\Phi^M = -ZF\left(\Phi^M - \Phi^s\right) = -ZF\Delta^M\Phi^S$$

That is:

$$\Delta^M\Phi^S = -\frac{\mu^M - \mu^s}{ZF} \tag{2}$$

where $\overline{\mu^M}$ and $\overline{\mu^s}$ are the pyrite (or galena) and solution electrochemical potential, respectively; μ^M is the chemical potential of the pyrite (or galena); μ^S is the chemical potential of reducible ions in solution; Φ^M and Φ^S are the inner potential of the pyrite (or galena) and the solution, respectively.

When the pyrite (or galena) is under elastic stress conditions, mechanical elements do not affect the electrolyte solution and the chemical potential of reducible ions in solution (μ^S) will not change, although the chemical potential of the pyrite (or galena) μ^M will change. The inner potential difference between the pyrite (or galena) and the electrolyte solution is written as:

$$\overline{\Delta^M\Phi^S} = -\frac{\overline{\mu}^M - \mu^s}{ZF} = -\frac{(\mu^M + VdP) - \mu^s}{ZF} = -\left[-\frac{\mu^M - \mu^s}{ZF}\right] - \frac{VdP}{ZF} = \Delta^M\Phi^S - \frac{VdP}{ZF}. \tag{3}$$

Solving the set of Eqs. (1)–(3), we obtain the electrode potential, which contains the residual stress:

$$\overline{\varphi_H^{MS}} = \overline{\Delta^M\Phi^S} - \Phi_0 = \left(\Delta^M\Phi^S - \frac{VdP}{ZF}\right) - \Phi_0 = \varphi_H - \frac{VdP}{ZF}. \tag{4}$$

The electrode potential difference for stress is:

$$\Delta\varphi_H^{MS} = \overline{\varphi_H^{MS}} - \varphi_H^{MS} = -\frac{VdP}{ZF}. \tag{5}$$

Eq. (5) shows that there is a negative linear relation between the pyrite (or galena) potential and the stress action. The experimental results shown in Fig. 6 are consistent with this electrochemical theory.

4.2. Galvanic interaction model

As electrically conducting sulfides minerals, when pyrite and galena are present in a medium that facilitates charge transfer, galvanic interaction occurs.

For the unstrained pyrite–galena galvanic, as Fig. 4 shows, galena (with the lower rest potential) dissolves anodically (Holmes and

Crundwell, 1995; Hackl et al., 1995; Hiroyoshi et al., 2002; Lu et al., 2000):

$$PbS \rightarrow Pb^{2+} + S^0 + 2e^-. \quad (6)$$

When sodium sulfate is the electrolyte, since sodium sulfate cannot be ionized oxidation-reduction ions, dissolved oxygen will be the only reactant on the pyrite cathode.

$$O_2 + 4H^+ + 4e^- \rightarrow 2H_2O. \quad (7)$$

When there is ferric sulfate in the electrolyte, due to its strong ionization, ferric sulfate and dissolved oxygen take part in reduction reactions on the pyrite cathode surface.

$$Fe^{3+} + e^- \rightarrow Fe^{2+}. \quad (8)$$

An unstrained pyrite–galena galvanic interaction model is shown in Fig. 8.

As relates to the strain energy residual of strained pyrite–galena galvanic, its electrode potential is lower than the galena electrode potential in the same solution system. This implies that strained pyrite–galena has a different interaction mechanism with the unstrained pyrite–galena galvanic cell. Strained pyrite (which has a lower rest potential) dissolves anodically (Langmuir, 1997; Williamson and Rimstidt, 1994):

$$FeS_2 + 8H_2O \rightarrow Fe^{2+} + 2SO_4^{2-} + 16H^+ + 14e^-. \quad (9)$$

Similarly to the unstrained pyrite–galena galvanic, a strained pyrite–galena galvanic interaction model is shown in Fig. 9.

4.3. Different Na^+ ion concentrations: experimental results and theoretical explanation

According to the galvanic interactions models in Figs. 8 and 9, whether for the unstrained pyrite–galena or the strained pyrite–galena galvanic, sodium sulfate only acts as a supporting electrolyte, while dissolved oxygen is the only reactant on the anode surface. Therefore if the sodium sulfate concentration is changed, the galvanic interaction corrosion current density and mixed potential will not obviously change. Rather, Fig. 4 shows that the galvanic corrosion current density and mixed potential fluctuated only mildly. This may be due to two causes: first, the dissolved oxygen quantity changed somewhat for the different sodium sulfate concentrations; second, before each experiment, the surfaces of the minerals were polished on metallographic paper, which may have caused the mineral surfaces to be different.

4.4. Different Fe^{3+} ion concentrations: experimental results and theoretical explanation

For the unstrained pyrite–galena galvanic, from the above discussion, O_2 participated in the galvanic interaction, but since the solubility of O_2 is very low (8–8.5 mg/L) at 25 °C and 1 atm, the limited current density of the cathode and the corrosion current density of the galvanic cell were likely very small (Hu, 1991); as a result, the

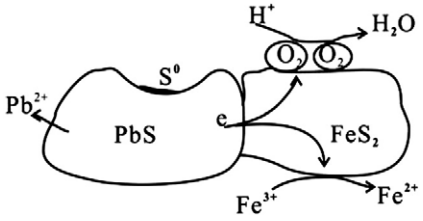

Fig. 8. The galvanic reaction model of the unstrained pyrite–galena couple.

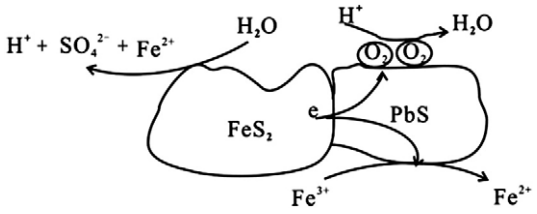

Fig. 9. The galvanic reaction model of the strained pyrite–galena couple.

existence of Fe^{3+} likely dominated the galvanic interactions due to its strong oxidizability, and the influence of dissolved oxygen on galvanic corrosion can be neglected. The Butler–Volmer equations of reactions (6) and (8), respectively, are presented below (Hu, 1991; Cao, 1985):

$$\begin{aligned} i_a = i_{PbS} &= i^0_{PbS}\left[\exp\frac{\alpha_{PbS}}{RT}\eta_a - \exp\left(-\frac{(1-\alpha_{PbS})}{RT}\eta_a\right)\right] \\ &= i^0_{PbS}\left[\exp\frac{\alpha_{PbS}}{RT}(E_g - E_{e,PbS}) - \exp\left(-\frac{(1-\alpha_{PbS})}{RT}(E_g - E_{e,PbS})\right)\right] \end{aligned} \quad (10)$$

$$\begin{aligned} i_c = i_{Fe^{3+}} &= i^0_{Fe^{3+}}\left[\exp\frac{\alpha_{Fe^{3+}}}{RT}\eta_c - \exp\left(-\frac{(1-\alpha_{Fe^{3+}})}{RT}\eta_c\right)\right] \\ &= i^0_{Fe^{3+}}\left[\exp\frac{\alpha_{Fe^{3+}}}{RT}(E_{e,Fe^{3+}} - E_g) - \exp\left(-\frac{(1-\alpha_{Fe^{3+}})}{RT}(E_{e,Fe^{3+}} - E_g)\right)\right] \end{aligned} \quad (11)$$

where i_a and i_c are the current densities of the anode and cathode, respectively; i^0_{PbS} and $i^0_{Fe^{3+}}$ are the exchange current densities of the PbS anode reaction and the Fe^{3+}/Fe^{2+} cathode reaction, respectively; E_g is the mixed potential of the galvanic cell; $E_{e,PbS}$ and $E_{e,Fe^{3+}}$ are the equilibrium potentials of the anode and cathode, respectively; α_{PbS} and $\alpha_{Fe^{3+}}$ are the transfer coefficients of the anode and cathode, respectively; R stands for the gas constant; F is the Faraday constant; and T is the absolute temperature.

As the corrosion galvanic interaction is a spontaneous oxidation-reduction process, it must be that $E_a < E_g < E_c$, and the corrosion potential E_g is far from both the anode equilibrium potential $E_{e,PbS}$ and the cathode equilibrium potential $E_{e,Fe^{3+}}$. Therefore, the anode oxidation and cathode reduction both have strong polarization, and the inverse processes of the electrode reactions can be neglected. Eqs. (10) and (11) can be simplified as:

$$i_a = i_{PbS} = i^0_{PbS}\exp\frac{\alpha_{PbS}F}{RT}(E_g - E_{e,PbS}) \quad (12)$$

$$i_c = i_{Fe^{3+}} = i^0_{Fe^{3+}}\exp\frac{\alpha_{Fe^{3+}}}{RT}(E_{e,Fe^{3+}} - E_g). \quad (13)$$

According to mixed potential theory, at the mixed potential E_g, the cathode current density i_c and the anode current density i_a are equal to the current density of the galvanic reaction i_g.

$$i_a = = -i_c = i_g. \quad (14)$$

Substituting Eqs. (12) and (13) into Eq. (14), we obtain the following equations:

$$E_g = \frac{\beta_a\beta_c}{\beta_a+\beta_c}\ln\frac{i^0_{Fe^{3+}}}{i^0_{PbS}} + \frac{\beta_a}{\beta_a+\beta_c}E_{e,Fe^{3+}} + \frac{\beta_a}{\beta_a+\beta_c}E_{e,PbS} \quad (15)$$

$$i_g = (i^0_{PbS})^{\frac{\beta_a}{(\beta_a+\beta_c)}}(i^0_{Fe^{3+}})^{\frac{\beta_a}{(\beta_a+\beta_c)}}\exp\left(\frac{E_{e,Fe^{3+}} - E_{e,PbS}}{\beta_a+\beta_c}\right) \quad (16)$$

where $\beta_a = \frac{RT}{\alpha_{PbS}F}$, $\beta_c = \frac{RT}{\alpha_{Fe^{3+}}F}$.

Holmes and Crundwell (1995) pointed out that an increase in ferric ions results in an increase in electrode potentials and equilibrium potentials of both the cathode and the anode; in addition, this will change the dynamic parameters for both half-reactions and increase the exchange current densities. Contrary to Eq. (15), we can clearly see that an increase in the concentration of ferric ions results in an increase in the mixed potential. The theoretical result is consistent with the experimental result shown in Fig. 5c.

The driving force behind the galvanic reaction is the difference between $E_{e,Fe^{3+}}$ and $E_{e,PbS}$, i.e. $E_{e,Fe^{3+}}-E_{e,PbS}$. From the above paragraph, we know that increasing the concentration of ferric ions makes the mixed potential more positive. The more positive potential is of greater advantage to the reduction of Fe^{3+} than the oxidation of PbS, thereby increase the driving force $E_{e,Fe^{3+}}-E_{e,PbS}$. From Eq. (16) we can see that when the concentrations of Fe^{3+} in the solution are enhanced, the corrosion current density of galvanic cells made of pyrite and galena will increase, consistent with the experimental results shown in Fig. 5a.

For the strained pyrite–galena galvanic, when there is Fe^{3+} in the solution, the following half-reaction occurs:

$$O_2 + 4H^+ + 4e^- \rightarrow 2H_2O \tag{7}$$

$$Fe^{3+} + e^- \rightarrow Fe^{2+} \tag{8}$$

$$FeS_2 + 8H_2O \rightarrow Fe^{2+} + 2SO_4^{2-} + 16H^+ + 14e^-. \tag{9}$$

The Butler–Volumer equations of the three reactions are shown as follows (Holmes and Crundwell, 2000):

$$i_{FeS_2} = k_{FeS_2}\left[H^+\right]^{-1/2}\exp\left(\frac{\alpha_{FeS_2}FE}{RT}\right) \tag{17}$$

$$i_{O_2} = -k_{O_2}[O_2]\left[H^+\right]^{0.14}\exp\left(\frac{-(1-\alpha_{O_2}FE)}{RT}\right) \tag{18}$$

$$i_{Fe^{3+}} = k_{Fe^{2+}}\left[Fe^{2+}\right]\exp\left(\frac{\alpha_{Fe}FE}{RT}\right) - k_{Fe^{3+}}\left[Fe^{3+}\right]\exp\left(\frac{-(1-\alpha_{Fe}FE)}{RT}\right) \tag{19}$$

where i is the corrosion current density, k is reaction rate constant, E is the electrode potential, α is the charge transfer coefficient, R is the universal gas constant, F is the Faraday constant, and T is the temperature.

In the presence of ferric ions and oxygen in the solution, the condition that produces a net balance of zero electrons is as follows:

$$i_{FeS_2} = -\left(i_{O_2} + i_{Fe}\right) = i_g. \tag{20}$$

Substituting Eqs. (17)–(19) into Eq. (20), and making the assumption that $\alpha_{FeS_2} \approx \alpha_{O_2} \approx \alpha_{Fe} = 1/2$, we obtain the following equations:

$$i_g = k_{FeS_2}\left[H^+\right]^{-1/2}\left(\frac{k_{Fe^{3+}}\left[Fe^{3+}\right] + k_{O_2}[O_2]\left[H^+\right]^{0.14}}{k_{Fe^{2+}}\left[Fe^{2+}\right] + k_{FeS_2}\left[H^+\right]^{-1/2}}\right)^{1/2} \tag{21}$$

$$E_g = \frac{RT}{F}\ln\left(\frac{k_{Fe^{3+}}\left[Fe^{3+}\right] + k_{O_2}[O_2]\left[H^+\right]^{0.14}}{k_{Fe^{2+}}\left[Fe^{2+}\right] + k_{FeS_2}\left[H^+\right]^{-1/2}}\right). \tag{22}$$

According to Henry's Law:

$$[O_2] = k_H \cdot P_{O_2} \tag{23}$$

where k_H is the Henry constant and P_{O_2} is the equilibrium pressure on the solution surface. In a 25 °C 1 atm open flow system, P_{O_2} is constant, so the concentration of dissolved oxygen $[O_2]$ is fixed. In addition, the experimental solution pH was 3.78. Contrasting Eqs. (21) and (22), we can conclude that the corrosion current density (i_g) and mixed potential (E_g) all increased as the Fe^{3+} ion concentration increased. Fig. 5b and d shows that the experimental results are consistent with the above analysis.

4.5. Different flow rates: experimental results and theoretical explanation

The galvanic current density for a flowing system can be described as follows (Zha, 2002):

$$i = \frac{n \cdot F \cdot D_j}{v_j} \cdot \frac{C_j^0 - C_j^s}{\delta_j} \tag{24}$$

where v_j, D_j and δ_j are the reaction coefficient, diffusion coefficient, and diffusion layer thickness of ion j; C_j^0 and C_j^S are the concentrations of ion j in the bulk solution and on the electrode surface, respectively; and n is the electron transfer number. Under flowing aqueous solution conditions, the diffusion layer thickness δ_j can be expressed as:

$$\delta_j = D_j^{1/3}\gamma^{1/6}y^{1/2}u_0^{-1/2} \tag{25}$$

where γ is the dynamic viscosity coefficient, y is the distance from a certain spot to the impact spot y_0, and u_0 is the flow rate of the solution.

From Eq. (25), we can see that the diffusion layer thickness δ_j is in direct proportion to $u_0^{-1/2}$, and that if the flow rate of the solution is enhanced, the diffusion layer thickness δ_j will become thinner. As Eq. (24) shows, the thinner the diffusion layer thickness δ_j, the larger the corrosion current density, which is consistent with the experimental results shown in Figs. 6a (b) and 7a (b). On the other hand, when the flow rate of the solution increases, the products on the electrode surface will be easily carried away; at the same time, the reactants will be brought more rapidly to the electrode surface, leading to intensified depolarisation and making the mixed potential positive, in agreement with the experimental results shown in Figs. 6c (d) and 7c (d).

5. Implications

(1) When two electrically conducting sulfide minerals are in contact with each other in a solution system, the mineral with the lower rest potential anodically dissolves while the one (with the higher rest potential) is protected. Therefore, when naturally-occurring pyrite, strained pyrite and galena were eroded, the chemical components of strained pyrite and galena were released first, while unstrained pyrite was galvanically protected by the adjacent strained pyrite and galena until all of the strained pyrite and galena disappeared. In the field of hydrometallurgy, it is acknowledged that the rest potential is the most crucial factor that affecting the hydrometallurgy progress. For a single sulfide mineral, a change in stress conditions can activate the rest potential, resulting in increased hydrometallurgy efficiency; however, when two sulfide minerals have close rest potential, the hydrometallurgy efficiencies are usually very low, by adding stress we can increase the difference in their rest potential and thereby increase the overall hydrometallurgy efficiency. In this point Dixon et al. (2007) had founded Galvanox process used galvanic coupling in a commercial process to leach chalcopyrite. They pointed that the Galvanox technology was a novel atmospheric leaching process which offers several potential advantages over existing copper-leach processes for primary copper sulfides. As it was selective for the primary sulfide mineral chalcopyrite over pyrite, it was applicable to low-grade or bulk concentrates. Copper recoveries of 98% or greater had been achieved in test work under controlled conditions, in periods of between 4 h and 24 h. Typically, about 90% of the concentrate was processed through the atmospheric leach tanks, with the remaining 10% being leached in a small pressure oxidation autoclave to provide heat and sulfuric acid make-up for the primary atmospheric leach.

(2) When the flow rate of a solution is below a critical velocity, the diffusion layer thickness is the same as the boundary layer thickness. A higher flow rate induces a more severe galvanic interaction. Surface, rain and underground water increase the heavy metals and acids produced, resulting in more serious environmental pollution in mining districts and the surrounding areas.

(3) It is well known that isolating oxygen is the most important way to stop sulfide oxidation. However, for unstrained pyrite–galena or the strained pyrite–galena couple, even without oxygen, the oxidizable metal ion Fe^{3+} in solution can act as a cathodic reducer, so the galvanic interaction will not be inhibited merely by isolating oxygen.

(4) In the future, by making use of the principles of the corrosion galvanic interaction, we may be able to use a Fe-bearing sulfide as the cathode of a chemical cell, with a piece of iron and steel scrap serving as the anode, to be inserted into acidic waste water discharged from an adjacent mine, with underground water as the loop. By applying an inverse voltage between the ore body and the scrap, we may be able to prevent the oxidation of sulfide minerals and the occurrence of galvanic interactions, and improve the acidic waste water discharged from mines, and thus control heavy metal pollution.

6. Conclusions

(1) Because of the strain energy residual of natural strained pyrite, its electrode potential is lower than potential of the galena electrode in the same solution system. This means that unstrained pyrite–galena and strained pyrite–galena galvanic cells undergo different interactions.

(2) Na^+ is a non-oxidizing and non-reducing ion, and does not take part in unstrained pyrite–galena and strained pyrite–galena galvanic interaction. Thus, even with an abundance of Na^+ ions, the corrosion current density and mixed potential will not noticeably obviously change.

(3) In the case of strongly oxidizing ions such as Fe^{3+} present in solution, the corrosion current density of unstrained pyrite–galena and strained pyrite–galena galvanic interaction will be greatly enhanced. At the same time, the higher the concentration of Fe^{3+} ions, the higher the corrosion current density and the more positive the mixed potential.

All of these facts indicate that oxidizing ions can speed up unstrained pyrite–galena and strained pyrite–galena galvanic interactions. This is an important means to improve the mine environment to reduce the discharge of Fe^{3+} and other strongly oxidizing ions.

(4) All else constant, the greater the flow rate, the higher the corrosion current density, indicating that the flow of surface water and mine-discharged water and the leaching of rain water can accelerate unstrained pyrite–galena and strained pyrite–galena galvanic interactions.

Acknowledgements

Many thanks should be extended to H. G. Xu and M. Q. Yang for their technical assistance in the experimental work. This work was financially supported by the National Natural Science Foundation of China (40573046; 40803017) and the Large-scale Scientific Apparatus Development Program of the Chinese Academy of Sciences.

References

Abraitis, P.K., Pattrick, R.A.D., Kelsall, G.H., Vaughan, D.J., 2003a. Acid leaching and dissolution of major sulfide ore minerals: process and galvanic effects in complex systems. In: Doyle, F.M., Kelsall, G.H., Woods, R. (Eds.), Electrochemistry in Mineral and Metals Processing, vol. VI. The Electrochemical Society Inc., pp. 143–153.

Abraitis, P.K., Pattrick, R.A.D., Kelsall, G.H., Vaughan, D.J., 2003b. In: Doyle, F.M., Kelsall, G.H., Woods, R. (Eds.), Electrochemistry in Mineral and Metals Processing, vol. VI. The Electrochemical Society Inc.

Akcil, A., Ciftci, H., 2003. Metals recovery from multimetal sulphide concentrates ($CuFeS_2$–PbS–ZnS): combination of thermal process and pressure leaching. Int. J. Miner. Process. 71 (1-4), 233–246.

Alpers, C.N., Blowes, D.W., 1994. Environmental Geochemistry of Sulfide Oxidation, vol. 550. American Chemical Society, Washington, DC.

Banfield, J.F., 1997. In: Nealson, K.H. (Ed.), Geomicrobiology: Interactions between Microbes and Minerals. ASM Press, Washington DC.

Cao, C., 1985. Principles of Corrosion Electrochemistry. Beijing, China.

Chandraprabha, M.N., Natarajan, K.A., Modak, J.M., 2004. Selective separation of pyrite–galena by biomodulation. Colloids Surf., B Biointerfaces 37 (3-4), 93–100.

Chernyshova, I.V., 2003. An in situ FTIR study of galena and pyrite oxidation in aqueous solution. J. Electroanal. Chem. 558 (30), 83–98.

Cruz, R., Sánchez, R., Lapidus, G.T., González, I., Monroy, M., 2005. An experimental strategy to determine galvanic interactions affecting the reactivity of sulfide mineral concentrates. Hydrometallurgy 78 (3-4), 198–208.

Dixon, D.G., Mayne, D.D., Baxter, K.G., 2007. "GALVANOX™—A Novel Process for Recovery of Copper from Primary Copper Concentrates," Copper 2007, the 6th International Conference, held in Toronto, Ontario, Canada.

Ekmekçi, Z., Demirel, H., 1997. Effects of galvanic interaction on collectorless flotation behaviour of galena and pyrite. Int. J. Miner. Process. 52 (1), 31–48.

Elliott, P., Ragusa, S., Catcheside, D., 1998. Growth of sulphate-reducing bacteria under acidic conditions in an upflow anaerobic bioreactor as a treatment system for acid mine drainage. Water Res. 32 (12), 3724–3730.

Hackl, R.P., Dreisinger, D.B., Peters, E., King, J.A., 1995. Passivation of galena during oxidative leaching in sulphate media. Hydrometallurgy 39 (1-3), 25–48.

Hiroyoshi, N., Arai, M., Miki, H., Tsunekawa, M., Hirajima, T., 2002. A new reaction model for the catalytic effect of silver ions on galena leaching in sulfuric acid solutions. Hydrometallurgy 63 (3), 257–267.

Holmes, P.R., Crundwell, F.K., 1995. Kinetic aspects of galvanic interactions between minerals during dissolution. Hydrometallurgy 39 (1-3), 353–375.

Holmes, P.R., Crundwell, F.K., 2000. The kinetics of the oxidation of pyrite by ferric ions and dissolved oxygen: an electrochemical study. Geochim. Cosmochim. Acta 64, 263–274.

Hu, M., 1991. Corrosion Electrochemistry. Beijing, China.

Huang, G., Grano, S., 2005. Galvanic interaction of grinding media with pyrite and its effect on flotation. Miner. Eng. 18 (12), 1152–1163.

Kelebek, S., Wells, P.F., Fekete, S.O., 1996. Differential flotation of galena, pentlandite and pyrrhotite in Ni–Cu sulphide ores. Can. Metall. Q. 35 (4), 329–336.

Langmuir, D., 1997. Aqueous Environmental Geochemistry. Prentice Hall, Upper Saddle River, NJ.

Lasaga, A.C., Blum, A.E., 1986. Surface chemistry etch pits and mineral–water reactions. Geochim. Cosmochim. Acta 50 (2), 363–379.

Li, D., 1999. Electrochemistry principle. Beijing, China.

Lu, Z.Y., Jeffrey, M.I., Lawson, F., 2000. An electrochemical study of the effect of chloride ions on the dissolution of galena in acidic solutions. Hydrometallurgy 56 (2), 145–155.

Majima, H., Peter, E., 1968. Electrochemistry of sulphide dissolution in hydrometallurgical systems. Leningrad.

Mckibben, M.A., Barnes, H.L., 1986. Oxidation of pyrite in low temperature acidic solutions: rate law s and surface textures. Geochim. Cosmochim. Acta 50 (1), 509–520.

Mehta, A.P., Murr, L.E., 1983. Fundamental studies of the contribution of galvanic interaction to acid-bacterial leaching of mixed metal sulfides. Hydrometallurgy 9 (3), 235–256.

Merkblatt ATV-DVWK M 153, 2000. Handlungsempfehlungen zum Umgang mit Regenwasser. GFA Gesellschaft zur FÖrderung der Abwassertechnik e.V., Hennef.

Natarajan, K.A., Iwasaki, I., 1972. Eh–pH response of noble metal and sulfide mineral electrodes. Trans. AIME 252, 437–439.

Pecina, E.T., Uribe, A., Finch, J.A., Nava, F., 2006. Mechanism of di-isobutyl dithiophosphinate adsorption onto galena and pyrite. Miner. Eng. 19 (9), 904–911.

Pecina-Treviño, E.T., Uribe-Salas, A., Nava-Alonso, F., Pérez-Garibay, R., 2003. On the sodium-diisobutyl dithiophosphinate (Aerophine 3418A) interaction with activated and unactivated galena and pyrite. Int. J. Miner. Process. 71 (1-4), 201–217.

Peng, Y.J., Grano, S., Fornasiero, D., John Ralston, J., 2003. Control of grinding conditions in the flotation of galena and its separation from pyrite. Int. J. Miner. Process. 70 (1-4), 67–82.

Rao, S.R., Finch, J.A., 1988. Galvanic interaction studies on sulphide minerals. Can. Metall. Q. 27 (4), 253–259.

Sato, M., 1992. Persistency-field Eh–pH diagrams for sulphides and their application to supergene oxidation and enrichment of sulphide ore bodies. Geochim. Cosmochim. Acta 56, 3133–3156.

Seke, M.D., Pistorius, P.C., 2006. Effect of cuprous cyanide, dry and wet milling on the selective flotation of galena and sphalerite. Miner. Eng. 19 (1), 1–11.

Sikka, D.B., Petruk, W., Nehru, C.E., Zhang, Z., 1991. Geochemistry of secondary copper minerals from Proterozoic porphyry copper deposit, Malanjkhand, India. Ore Geol. Rev. 6 (2-3), 257–290.

Thornber, M.R., 1975a. Supergene alteration of sulphides II. A chemical study of the Kambalda nickel deposits. Chem. Geol. 15, 137–176.

Thornber, M.R., 1975b. Supergene alteration of sulphides I. A chemical model based on massive nickel sulphide deposits at Kambald, Western Australia. Chem. Geol. 15, 1–14.

Williamson, M.A., Rimstidt, J.D., 1994. The kinetics and electrochemical rate-determining step of aqueous pyrite oxidation. Geochim. Cosmochim. Acta 58, 5443–5454.

Zha, Q.X., 2002. Introduction to Dynamics of Electrode Processes, (3rd edition). Beijing, China.

Zhang, Q., Xu, Z., Bozkurt, V., Finch, J.A., 1997. Pyrite flotation in the presence of metal ions and sphalerite. Int. J. Miner. Process. 52 (2-3), 187–201.